BIOCHEMISTRY
including biophysical chemistry & molecular biology
Article

Biochemistry **2010,** *49,* 3031–3039 3031
DOI: 10.1021/bi901444w

Simultaneous Single-Molecule Fluorescence and Conductivity Studies Reveal Distinct Classes of Aβ Species on Lipid Bilayers[†]

Joseph A. Schauerte,*[,‡,§] Pamela T. Wong,[‡] Kathleen C. Wisser,[§] Hao Ding,[§] Duncan G. Steel,[§,∥] and Ari Gafni[‡,§]

[‡]*Department of Biological Chemistry,* [§]*Department of Biophysics, and* [∥]*Department of Electrical Engineering and Computer Sciences, University of Michigan, Ann Arbor, Michigan 48109*

Received August 17, 2009; Revised Manuscript Received February 15, 2010

ABSTRACT: The extracellular senile plaques prevalent in brain tissue in Alzheimer's disease (AD) are composed of amyloid fibrils formed by the Aβ peptide. These fibrils have been traditionally believed to be featured in neurotoxicity; however, numerous recent studies provide evidence that cytotoxicity in AD may be associated with low-molecular weight oligomers of Aβ that associate with neuronal membranes and may lead to membrane permeabilization and disruption of the ion balance in the cell. The underlying mechanism leading to disruption of the membrane is the subject of many recent studies. Here we report the application of single-molecule optical detection, using fluorescently labeled human Aβ40, combined with membrane conductivity measurements, to monitor the interaction of single-oligomeric peptide structures with model planar black lipid membranes (BLMs). In a qualitative study, we show that the binding of Aβ to the membrane can be described by three distinctly different behaviors, depending on the Aβ monomer concentration. For concentrations much below 10 nM, there is uniform binding of monomers over the surface of the membrane with no evidence of oligomer formation or membrane permeabilization. Between 10 nM and a few hundred nanomolar, the uniform monomer binding is accompanied by the presence of peptide species ranging from dimers to small oligomers. The dimers are not found to permeabilize the membrane, but the larger oligomers lead to permeabilization with individual oligomers producing ion conductances of < 10 pS/pore. At higher concentrations, perhaps beyond physiologically relevant concentrations, larger extended and dynamic structures are found with large conductances (hundreds of picosiemens), suggesting a major disruption of the membrane.

One of the hallmarks of Alzheimer's disease (AD) is the formation of insoluble neurofibrillary tangles and senile plaques in brain tissue. The major component of these proteinaceous plaques is the 39−43-amino acid Aβ peptide, derived by proteolytic cleavage of the membrane-spanning amyloid precursor protein (APP). The mechanism that underlies the pathogenicity of Aβ toward neuronal tissue is the subject of intense research.

In vitro studies of Aβ reveal that in aqueous solution the peptide progressively associates from its monomeric form via low-molecular weight species to extended β-sheet fibrils, a process that is highly dependent upon experimental conditions (*1*, *2*). It was originally assumed that Aβ becomes cytotoxic when it forms these large insoluble fibrillar aggregates (*3*, *4*), historically termed the amyloid hypothesis. For the purposes of this paper, we use the term cytotoxic to mean that Aβ causes deviations from the cell's normal healthy homeostasis that relate to the disease (i.e., Alzheimer's) and/or possibly cell death.

In contrast with the amyloid hypothesis, recent studies have demonstrated that cytotoxicity might be associated with small oligomers of Aβ that bind to the neuronal membrane, leading to cell death possibly by membrane permeabilization (*5*−*9*). In the generalization of this hypothesis, it has been suggested that other amyloid-associated diseases share this mechanism of cell toxicity, where peptide-generated disruption of the membrane (possibly producing well-defined pores) allow an unrestricted influx of ions such as Ca^{2+} into cells, thereby stressing them either directly (*10*−*18*) or indirectly by triggering Ca^{2+} sensitive apoptosis signaling pathways (*15*, *19*−*21*). A number of studies have tested this hypothesis through cell viability assays (*20*, *22*−*24*), permeability studies using liposomes (*25*−*27*), and conductivity studies using lipid bilayers (*8*, *28*−*31*).

Efforts to identify membrane-permeabilizing structures formed by amyloidogenic peptides have utilized a variety of techniques, including atomic force microscopy (*17*, *19*, *32*−*34*), electron microscopy (*9*, *35*, *36*), and conductivity measurements (*31*, *37*−*40*). A causal relationship between small oligomers of Aβ and toxicity has been hypothesized from these studies, but efforts to develop a more detailed mechanistic understanding of how Aβ assembles into toxic species and of the basis of the toxicity have been limited by significant experimental challenges since under physiologically relevant conditions the Aβ aggregates are metastable, present at extremely low concentrations, and highly heterogeneous. These features make it very difficult to detect and characterize the different structures as they form and to monitor their integration into the membrane, thereby further hampering detailed mechanistic studies. Thus, in spite of many efforts, the identification of the toxic species and the specific mechanism by which they inflict toxicity has proven to be difficult (*22*, *28*, *34*, *41*−*44*).

In this work, we present results of a single-molecule study of Aβ binding to a model planar black lipid membrane (BLM)[1]

[†]This research was supported by National Institute on Aging Grant R21 AG027370 and the Michigan Alzheimer's Disease and Research Center.

*To whom correspondence should be addressed: Department of Biophysics, Chemistry Building, 930 N. University, Ann Arbor, MI 48109. E-mail: schauert@umich.edu. Phone: (734) 936-2111. Fax: (734) 764-3323.

[1]Abbreviations: Aβ40, Aβ 1−40; Aβ42, Aβ 1−42; APD, avalanche photodiode; BLM, black lipid membrane; DiphPC, diphytanoylphosphatidylcholine; DiphPS, diphytanoylphosphatidylserine; FRAP, fluorescence recovery after photobleaching; HL488, Hilyte 488 fluorophore; SMH, Shai−Matsuzaki−Huang; ThT, thioflavin T.

Published on Web 03/04/2010

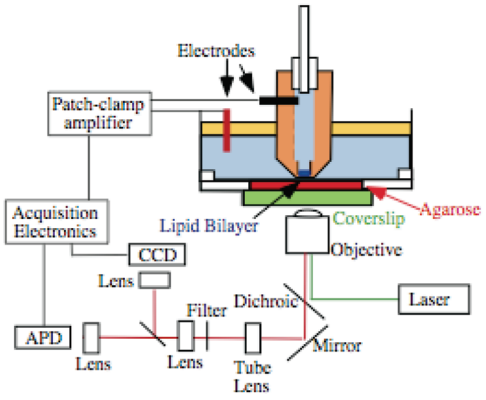

FIGURE 1: Single-molecule BLM system comprised of an in-house built inverted confocal microscope utilizing an Olympus 60× 1.45 NA objective. Frequency-doubled Ti:sapphire output was used for single-photon excitation of fluorescently labeled HL488 Aβ bound to the surface of the black lipid membrane. Images were recorded by raster scanning the surface of the BLM with a piezo-electric stage with emission detected by an avalanche photodiode. A CCD camera was used to determine that oligomeric structures were within the area to be raster scanned. The maximum resolution is set by the diffraction limit, approximately 0.5 μm. Ag/AgCl electrodes measure current through the BLM bilayer formed on the surface of agarose layered on the coverslip.

system. Using fluorescently labeled Aβ combined with the ability to measure membrane electrical conductance, we show that Aβ binding and membrane permeabilization in this system fall into three distinct morphological classes. (1) At relatively low peptide concentrations (< 10 nM), we find uniform binding of Aβ to the membrane surface that involves monomers only with no detectable membrane conductance (< 1 pS). (2) At intermediate peptide concentrations, between 10 nM and several hundred nanomolar, we find small oligomers (from dimers to ~14mers), where the dimers produce no detectable conductance but the larger oligomers result in conductance values of < 10 pS per oligomer. (3) At the highest peptide concentrations (≫100 nM), we find large structures of Aβ that slowly move across the surface and are associated with large electrical conductivity (approximately hundreds of picosiemens). From the data, we conclude that the interactions of Aβ with the membrane surface are highly nonlinear with respect to peptide concentration and that if this behavior occurs on the surface of neurons the toxicity, if due to permeabilization, would depend profoundly on the intracellular Aβ concentration.

MATERIALS AND METHODS

SMS Conductivity System. Figure 1 shows the experimental setup used to measure membrane conductivity and single-molecule fluorescence simultaneously. This system is comprised of an in-house built inverted confocal microscope utilizing an Olympus 60× 1.45 NA objective. The output of an 80 MHz Coherent Ti:Saphire laser is frequency doubled to 460 nm (Inrad, Northvale, NJ) and used for single-photon excitation of fluorescently labeled Aβ bound to the surface of the black lipid membrane (BLM). A Chroma (Rockingham, VT) Q500XRU dichroic filter is used to separate excitation and HL488 emission. Images are recorded by raster scanning the surface of the BLM with a piezo-electric stage (Physik Instrumente, Auburn, MA) with emission detected by an avalanche photodiode (APD) (EG&G Ortec SPCM-AQR-16). A CCD camera was used to determine that all oligomeric structures were within the area to be raster scanned. The maximum resolution is set by the diffraction limit, approximately 0.5 μm. Ag/AgCl electrodes measure current through the BLM bilayer formed on the surface of agarose layered on the coverslip.

Black Lipid Membranes. BLMs were generated using a 70/30 solution of diphytanoylphosphatidylcholine and diphytanoylphosphatidylserine (DiphPC/DiphPS) (Avanti Polar Lipids, Alabaster, AL) in methylcyclohexane. The membrane was formed by the procedure outlined by Ide et al. (*45*), in which an aqueous solution of Aβ is covered by cyclohexane containing 10 mg/mL lipids. The interface between the phases has a multilamellar membrane that is forced by the probe onto an agarose surface coating the microscope coverslip to form a unilamellar membrane under very low hydrostatic pressure within the probe channel. Formation of a single bilayer was monitored by membrane capacitance (~1 μF/cm^2) utilizing the Warner 535 patch clamp amplifier.

Bilayer Conductivity Measurements. BLM conductance was monitored with a Warner (Hamden, CT) DG535 bilayer voltage amplifier, with digitization and data acquisition using home-written software and a National Instruments 6070 AD card using Labview. Analysis was performed by a procedure utilizing Igor Pro analysis routines. A four-pole Bessel filter was applied to the signal to improve the signal-to-noise ratio. The Ag/AgCl electrodes were chlorinated by a 30 min treatment with bleach.

Aβ *Sample Preparation*. Salts and buffers were obtained from Sigma-Aldrich (St. Louis, MO). Fluorescently labeled and unlabeled Aβ40 were obtained from Anaspec (San Jose, CA). Fluorescently labeled Aβ40 was N-terminally labeled with Hilyte 488 (Aβ40-HL488) by Anaspec. Aβ40 was distributed into smaller aliquots by being dissolved as a lyophilized powder in 1% ammonium hydroxide, sonicated for 1 min, then relyophilized into 20 μg samples. Aβ was then dissolved at 50 μM in distilled water, vortexed for 1 min, and then brought to a concentration of 25 μM with 2× buffer, resulting in a final buffer that consisted of 5 mM sodium phosphate and 100 mM sodium chloride (pH 7.4). Final peptide concentrations between 1 nM and several hundred nanomolar were produced by further dilution with buffer.

Fluorescence Lifetime Measurements. Time-correlated single-photon counting measurements (TCSPC) were taken using standard procedures (*46*) in reverse counting mode. A Coherent Verdi V-10 diode laser pumped a Coherent model Mira 900 Ti:Sapphire laser (Santa Clara, CA) operating with a pulse width of 150 fs. The output was frequency-doubled using an Inrad (Northvale, NJ) model 5-050 Ultrafast Harmonic Generating system. The excitation rate was 4 MHz, controlled by a Coherent 9200 Pulse Picker. Fluorescence emission was detected with either a Hamamatsu (Bridgewater, NJ) R3809U-50 microchannel plate photomultiplier or a Hamamatsu H7421 photomultiplier input into a Tennelec (Oak Ridge, TN) quad Constant Fraction Discriminator (model TC455). Analog output from an Ortec (Oak Ridge, TN) time−amplitude converter (model 457) was digitized by a system developed in our laboratory utilizing National Instruments hardware (NI6070 12 bit A/D converter, NI6602 counter) and controlled by Labview Software (S. Parus, Department of Chemistry, University of Michigan) that simultaneously records total emission and fluorescence anisotropy. Anisotropy measurements utilized a Hinds (Hillsboro, OR) PEM-90 photoacoustic modulator to monitor horizontal and vertical polarizations at 42 kHz. Time-resolved studies with

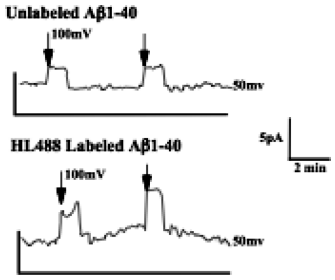

FIGURE 2: Conductivity plots for 100 nM unlabeled Aβ40 and Hilyte 488-labeled Aβ40 added to a BLM after a 4 h incubation in buffer at 20 °C. The BLM was maintained at a potential of 50 mV with transient changes to a potential of 100 mV (arrows).

BLMs also utilized a Picoquant (Berlin, Germany) Timeharp 200 card running at an excitation rate of 80 MHz.

RESULTS

Identification of Membrane-Permeabilizing Aβ Structures. To identify membrane-bound structures produced by Aβ and quantify their associated membrane permeabilization efficacy, we utilized Aβ40 that had been fluorescently labeled with Hilyte 488 (Anaspec) and applied single-molecule optical detection to monitor individual peptide oligomers bound to the BLM while simultaneously determining the electrical conductivity associated with the same sample.

Our experimental setup, shown in Figure 1, provides the capability to individually image labeled Aβ oligomers on the surface of a 50 μm radius BLM and correlate the optical image with the integrated conductivity of the membrane. To confirm that peptide labeling with the fluorescent dye has not altered its membrane permeabilizing behavior, both labeled and unlabeled peptides (100 nM) were incubated for 4 h in an aqueous solution, and each was then added (separately) to the membrane preparations. Conductivity was monitored (Figure 2), and the results confirm that the labeled Aβ-HL488 preserves the membrane permeabilizing capability of the unlabeled peptide. There is substantial variability in BLM conductivity with both unlabeled and labeled Aβ between different sample preparations with no apparent differences in the protocol. This effect, coupled with the limited stability of BLMs (tens of minutes in the absence of Aβ peptide), makes quantitative studies challenging at this point. Thus, while we observe that both labeled Aβ peptide and unlabeled Aβ peptide affect membrane permeabilization with comparable conductivities and time scales, a more detailed comparison of the relative permeabilizing ability of labeled and unlabeled peptides has not yet been accomplished.

A direct way to evaluate the number of labeled Aβ molecules in a given membrane-bound oligomer is by counting the number of steps observed when the oligomer is photobleached by the laser light. While we have used this approach in the past (*47*), we found it to be inadequate for this study since some of the peptide under study is rapidly diffusing and these species are present in all the BLM raster scanned surfaces where they provide a fluorescence background. This makes the determination of oligomer size by the bleaching technique impractical since during a bleaching experiment the constant infusion of new background fluorescence creates an uninterpretable bleaching profile. In addition, as the oligomers become larger, they also become progressively more difficult to analyze for size by photobleaching, since the relative size of individual bleaching steps diminishes.

Estimating the size of an oligomer from its fluorescence intensity relative to that of a monomeric species was also not adequate since we found the fluorescence to be progressively quenched as oligomers grew. To evaluate an oligomer's size, therefore, we used the lifetime-normalized fluorescence intensity and compared the oligomer's fluorescence intensity (F) and its associated fluorescence lifetime (τ) to those of individual HL488 dye molecules adsorbed on glass. The number of peptides in the oligomer (N) was calculated as

$$N = (F_{\text{oligomer}}/F_{\text{dye}})(\tau_{\text{dye}}/\tau_{\text{oligomer}})$$

We observed that discrete species with up to 18−20 peptides do not require lifetime normalization (i.e., have an intrinsic lifetime of the dye), while the extended structures can have highly attenuated lifetimes.

A wide-field CCD camera was used to verify that all the fluorescent species detected were contained within the raster scanned area, and an example of oligomer size determination using the equation given above is presented in Figure 3A. At an excitation power of 5 μW and a diffraction-limited beam profile, a single Hilyte 488 dye molecule yields a mean value of 9000 ± 2000 counts per second above background with a fluorescence lifetime of 4.1 ns. The intensity of the prominent fluorescence peak observed in Figure 3A (16000 cps; its value adjusted via subtraction of the fluorescence background due to rapidly diffusing species) was divided by the intensity observed for the single dye molecule (9000 cps), resulting in a species that most closely represents a dimer of Aβ. For this experiment, the dimer had the same lifetime as the free dye in ensemble measurements or when isolated on a glass surface (or as a monomer on the membrane); $\tau_{\text{dye}} = 4.1 \pm 0.15$ ns.

Experiments that aim to characterize interactions of Aβ-HL488 with the phospholipid membrane revealed three distinct classes of bound peptide species, as depicted in Figure 3B−F: (1) small, monomeric, species that are homogeneously distributed throughout the membrane surface (Figure 3B), (2) small, but discrete, oligomers seen as fluorescent spikes in Figure 3C−E, and (3) spatially extended structures whose size is above the diffraction limit, as seen in Figure 3F.

The class 1 Aβ species is present in all the samples shown in Figure 3B and produces an elevated fluorescence background (red surface) over that of peptide-free membrane samples (blue surface) that arises from monomeric peptide binding and freely diffusing across the membrane surface. This elevated fluorescence is evenly distributed across the membrane surface, is stable for a period of several hours, and does not change membrane conductivity, which remains at the basal level (< 0.3 pS). This result suggests that Aβ binding promotes membrane stabilization.

The lifetime-normalized fluorescence intensity of the class 1 membrane-bound Aβ-HL488 shown in Figure 3B corresponds to five monomers of the labeled peptide per square micrometer. Assuming a surface area of ~70 Å^2 per lipid molecule, we calculate a lipid/peptide ratio of ca. 2.8×10^5. Hence, only a small fraction of the lipid appears to be actively binding the Aβ. Analysis of the fluorescence intensity from unit areas of 0.5 μm^2, done across the 40 μm × 40 μm surface shown in Figure 3B, reveals intensity variations that are only marginally above those expected for Poisson statistics, which is consistent with a uniform distribution of monomeric fluorophores. The diffusion constant of Aβ40-HL488 on a POPC/PG model membrane is 2.3 μm^2/s (H. Ding et al., manuscript in preparation), which we determined

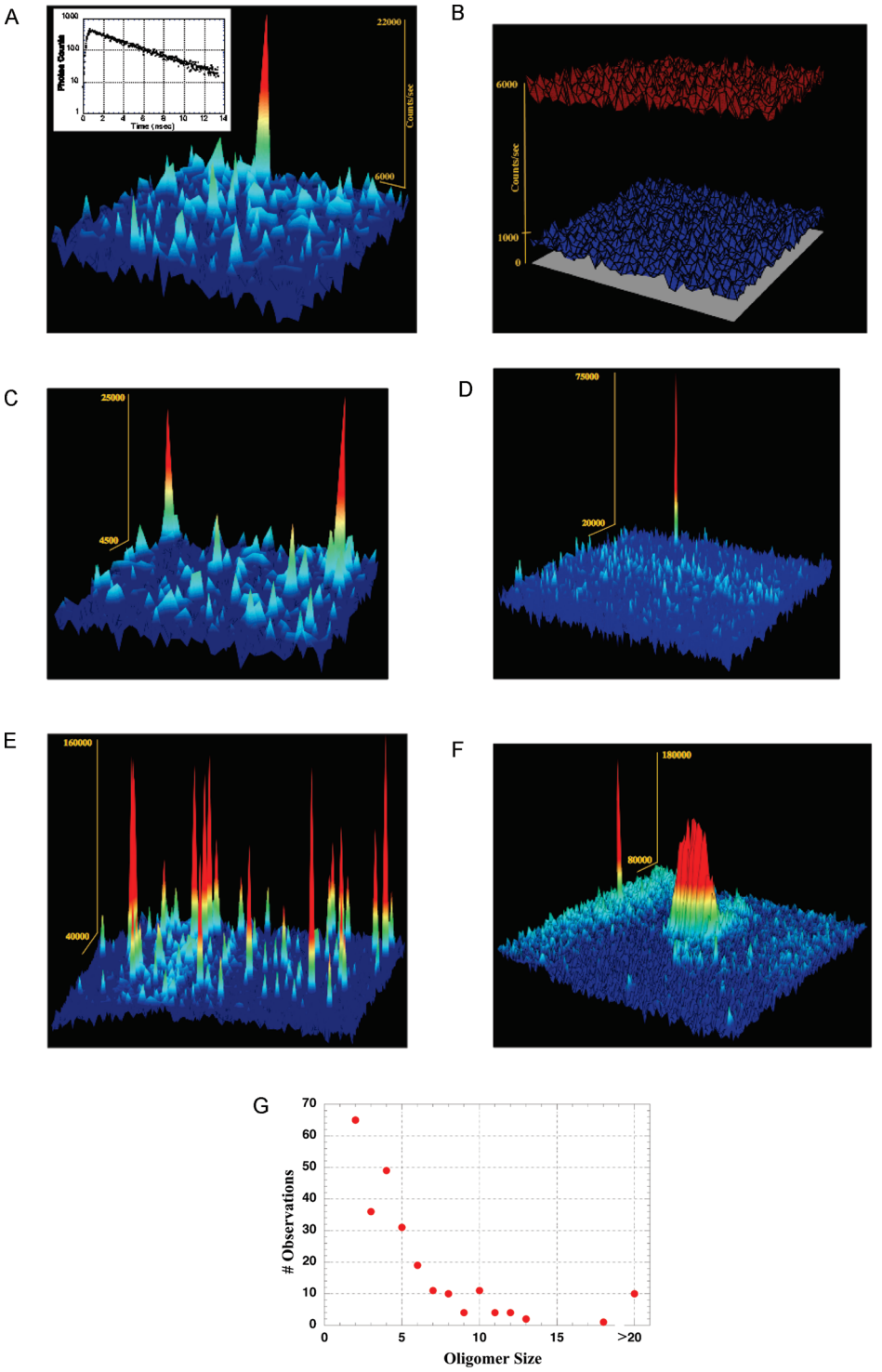

FIGURE 3: Examples of membrane-bound Aβ species. The panels show the fluorescence images (linear scale of counts per second) obtained by scanning the BLM surface with 460 nm excitation and monitoring through a 500 nm dichroic filter. The resolution in these 40 μm $\times$ 40 μm scanned areas is near the diffraction limit ($\sim$0.5 μm). The emission intensity and fluorescence lifetime of an individual HL488 dye molecule are used to assess the number of fluorescently labeled Aβ molecules associated with discrete pores on the BLM surface. In the case of pores observed in this figure, the fluorescence lifetime has been within 10% of the lifetime of the free chromophore. On the basis of these numbers, we estimate that the structure on the BLM in panel A contains a single peak with two monomers and has a conductivity of <0.3 pS (i.e., below our detection limit). Rescanning of this surface indicated this peak exhibited a diffusion rate below the current measurement limit of 5×10^{-4} μm^2/s. (B) Nonconducting BLM surface with membrane-bound Aβ40-HL488. The average fluorescence intensity corresponds to approximately four or five dye molecules per square micrometer of surface area (top red surface). The bottom surface (blue) shows the background from the BLM in the absence of labeled Aβ40-HL488. (C) Two distinct, small, oligomers. On the basis of the lifetime-normalized fluorescence intensity, both most closely matched Aβ dimers. No membrane conductivity was detected. (D) Example of a single-membrane permeabilizing oligomer with a conductivity of 2 pS. The lifetime-normalized fluorescence intensity corresponds to that of an Aβ hexamer. (E) Several discrete structures are observed with a total conductivity of 80 pS, and the most intense fluorescence peaks correspond to structures with approximately 12−14 dye molecules. (F) At 250 nM labeled Aβ40-HL488, extended and discrete structure coexist on the membrane. The total conductivity is 150 pS. (G) Histogram of 257 discrete species, including 103 species observed without corresponding conductivity data. The data at a size of 20 oligomers represent those of species with more than 20 peptides.

by incubating 50 nM Aβ with the membrane, washing the solution peptide off, and then performing a FRAP measurement. This is consistent with a rapid movement of labeled Aβ leading to homogeneous fluorescence intensity in our 50 ms raster scanned data. Our observations support a model in which monomeric Aβ binds to the membrane with high affinity and is delocalized to form a rapidly diffusing uniform layer (at a low peptide/lipid ratio) but does not induce measurable conductivity (above a background of 0.3 pS). It should be noted that in the work of Ding et al. (manuscript in preparation) incubation of POPC/PG membranes at higher Aβ40-HL488 concentrations also resulted in discrete and immobile fluorescence species consistent with these observations on agarose-supported BLM surfaces. High-affinity binding of Aβ1−40 to model membranes has also been reported by Kremer and Murphy (*48*).

Examples of class 2 Aβ oligomers are shown in Figure 3C−E revealing fluorescent species that most closely match two dimers (C), a hexamer (D), and many oligomers (E). These discrete membrane-bound species are all below the optical diffraction limit; however, using their lifetime-normalized fluorescence intensities, we conclude that dimeric Aβ exhibits no conductivity. The smallest structure that we observed to possess a detectable conductivity [~2 pS (Figure 3D)] is approximately a hexamer. While systematic errors (e.g., steric hindrance of complete rotational averaging, partial static quenching, etc.) could modify this number somewhat, we note that structures of comparable size resembling pores, composed of Aβ peptides, have been previously detected by AFM (*17*), though those structures could not be tested for membrane interaction or permeabilization. We further note that we observe conductivity only when we simultaneously observe immobilized oligomers with more than five to eight monomers. We note that even the nonconducting dimer shown in Figure 3A is effectively immobilized (with a diffusion constant below the current measurement limit of 5×10^{-4} μm^2/s). The dramatically reduced mobility of these species may be associated with interactions of the oligomers with the underlying agarose surface. Finally, we note that these data are in reasonable agreement with the Aβ40 oligomer size of six to eight monomers in the model proposed by Arispe et al. (*8*).

Interestingly, recent work by Selkoe's group (*49*) shows that the dimeric and possibly trimeric (*50*) forms of Aβ leads to modified plasticity of the synaptic junction in neuronal cells. While we can only quantitate membrane permeabilization by relatively larger oligomers, it is possible that the dimeric species aggregates on the neuronal membrane to form larger, and toxic, oligomers. While neuronal toxicity may arise from mechanisms other than membrane permeabilization (the property determined in our experiments), this hypothesis is supported by the observation that Aβ both permeabilizes the cell, allowing the influx of calcium, and, by some mechanism, causes cell death as discussed above. We also note that our membrane system is a simplified model for the neuronal membrane and may not fully represent the latter's behavior.

It is also interesting to note that we observe significant heterogeneity in the size and conductance of these small membrane-bound oligomers. For example, some of the structures shown in Figure 3E correspond to 12−14 dye molecules, and from the total conductivity of 80 pS, we estimate that each of these possesses a higher conductivity than the structures in Figure 3D. The data clearly show the existence of multiple types of conducting Aβ oligomeric structures.

When higher Aβ concentrations ($\gg$100 nM) were incubated with the BLM, we observed a new, much larger, lipid-bound peptide species, denoted above as class 3. Figure 3F shows a membrane surface after incubation for a few minutes with 250 nM Aβ40-HL488 revealing large areas of disrupted membrane (well beyond the diffraction limit) that evolve in time and that exist simultaneously with discrete (class 2) structures of Aβ on the membrane. The combined membrane conductivity of this sample was 150 pS, and that is clearly mostly due to the extended structure. The observation that the two Aβ oligomer types can coexist on the BLM indicates that conditions for generating these disparate species are not mutually exclusive. A histogram of the size of the discrete structures is illustrated in Figure 3G (including 103 species without corresponding conductivity data). One can see that the larger oligomer species are increasingly less common.

The small, class 2, Aβ structures are static and do not change over several hours. We have on occasion observed that the discrete species remain intact after 16 h. The BLM stability is dependent upon the characteristics of the Teflon probes used to form the membranes. However, we have consistently observed that the extended class 3 structures are dynamic and can evolve with time. This is demonstrated by the progression seen in the consecutive scans in Figure 4A and in the corresponding evolution of conductivity shown in Figure 4B. Here, 1 μM Aβ40-HL488 was incubated for several minutes with the BLM. The initial scan in Figure 4A is associated with a average membrane conductance of 230 pS, while in the subsequent scans, taken over the following 30 min, the fluorescence profile evolves and changes in several locations on the membrane. The overall conductance significantly increases until the membrane is entirely disrupted and the conductivity reading is off scale, which occurs at the very termination of Figure 4B (after the final scan in Figure 4A was completed). The heightened fluorescence intensity of the extended structures is generally associated with shortened fluorescence lifetimes (< 1 ns compared to 4.1 ns for small HL488 Aβ oligomers), which may reflect a different environment for the HL488 or be the result of efficient intra-aggregate energy transfer due to closer positioning of the fluorophores.

To complement the measurements with fluorescence-labeled Aβ, we performed experiments using ThT that fluoresces upon binding to the β-structure of fibrils. To study the evolution of these structures in ensemble measurements, we use panels A and B of Figure 5 to show ensemble steady state and time-resolved fluorescence and fluorescence anisotropy measurements of ThT bound to Aβ40 that has been incubated for different lengths of time in solution. ThT was added to freshly solubilized Aβ40 at 1 μM, and the sample was then incubated for 4, 22, and 46 h at 37 °C in 10 mM sodium phosphate and 100 mM sodium chloride (pH 7.4). Initially, for ThT added to freshly solubilized 1 μM Aβ40, the Aβ40 has a fluorescence lifetime of 30 ps that is indistinguishable from that of free ThT (data not shown). During incubation, the steady state ThT fluorescence is progressively enhanced and the fluorescence lifetime becomes broadly distributed, indicative of a heterogeneous mixture. The fluorescence polarization anisotropy indicates binding to a species with a rotational correlation time of ~15 ns, quite distinct from that of monomeric Aβ40 in solution (~5 ns) and corresponding to oligomers with molecular masses in the range of 25−40 kDa. Further incubation of the peptide in solution (for 46 h) shows ThT binding to a species with a very long rotational correlation time (> 50 ns, the upper limit of the operating conditions of the instrument) consistent with a large (fibrillar) structure(s). Aβ40 incubated for long periods of time has an attenuated ability to

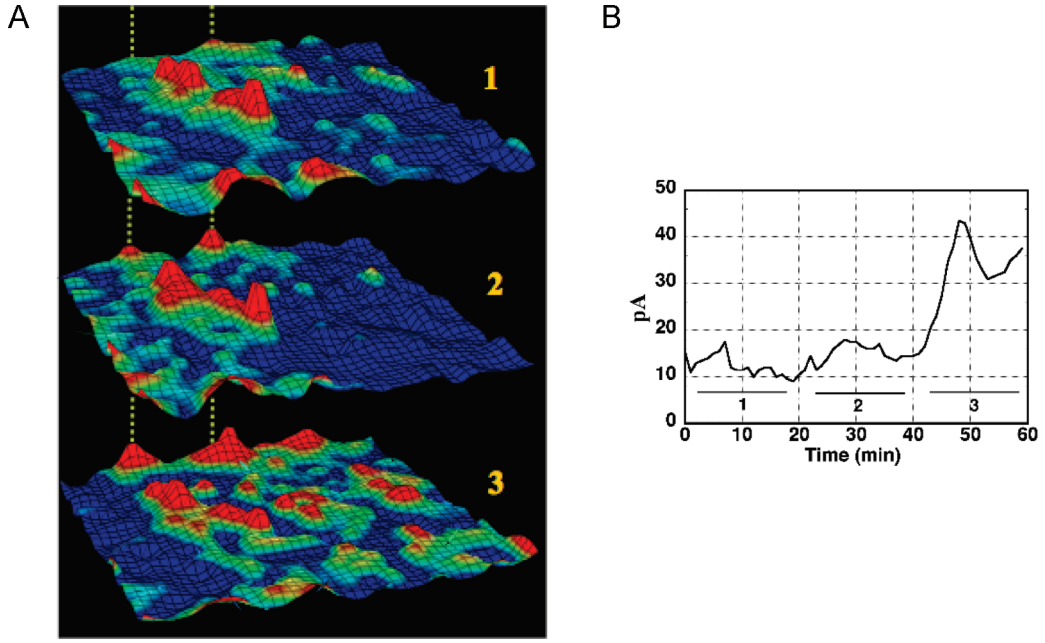

FIGURE 4: Time progression of extended pore structures. Aβ40-HL488 (1 μM) was incubated with the BLM and formed extended pore structures that were dynamic in time. Raster scans of the 40 μm × 40 μm BLM surface were initiated at approximately 1, 22, and 42 min (corresponding to solid lines labeled 1−3, respectively, in panel B) with a holding potential of 50 mV and show BLM surfaces with conductivities averaging (1) 230, (2) 280, and (3) 600 pS, respectively. The dashed lines in panel A indicate regions that underwent significant evolution in surface morphology. These membranes often disintegrate when the conductivity exceeds several nanosiemens for a 50 μm radius BLM. Since our resolution of conductivity is nominally 0.3 pS, the variation seen in panel B represents real changes in BLM conductivity. While some changes in fluorescence lifetime have been noted in the extended structures, it is not presently clear how much the intensity increase is associated with changes in the fluorescence quantum yield or increased concentration of labeled Aβ40-HL488.

form membrane permeabilizing pore structures, as most of the peptide is incorporated into fibrils.

Figure 5C is intended to complement the higher-concentration data in Figure 4, showing data obtained with unlabeled Aβ40 incubated in the presence of ThT. The results were obtained with a freshly dissolved 100 nM Aβ40 sample interacting with the BLM for 10 min in the presence of 5 μM ThT. Discrete ThT-stained species are detected by their fluorescence, and the resultant permeabilization leads to a total BLM conductivity of 20 pS. The ThT fluorescence shows that the binding of Aβ to the model membrane leads to formation of β-structure. Furthermore, given the concentration and conductivity, we believe this may correspond to some of the small structures seen with fluorescently labeled Aβ in Figure 3C−E.

From the results presented above, we conclude that interaction of Aβ with the phospholipid membrane greatly accelerates formation of oligomer and β-structure (both appear within minutes compared to hours in solution). It is possible, then, that both the small, class 2, and extended, class 3, peptide aggregates bind ThT and therefore are likely to contain at least some β-structure.

DISCUSSION

The association of Aβ with lipid membranes is driven by a combination of electrostatic and hydrophobic interactions (*26*, *51*). Monomeric Aβ in solution is predominantly disordered (*1*, *2*) but develops increasing amounts of secondary structure upon binding to negatively charged lipids (*26*, *51*). Recent work in our laboratory using circular dichroism in ensemble studies (*52*) indicates that at low protein/lipid ratios (< 1/50) Aβ assumes a mostly α-helical conformation while higher protein/lipid ratios induce a transition to β-sheet conformation. At the low protein/lipid ratios, the α-helical structure is supported by the interaction of positively charged residues of amphipathic α-helices with negatively charged lipids (*53*), while at higher Aβ/lipid ratios, the β-sheet structure is stabilized by protein−protein interactions on the membrane surface. At moderate peptide concentrations, free diffusion on the membrane surface and association of α-helical monomers support the formation of oligomers that can then adopt a new conformation capable of permeabilizing the lipid membrane (*54*, *55*). This model suggests that membrane permeabilizing species can be generated by lipid-induced conformational changes in Aβ followed by additional peptide−peptide interactions inducing further structural rearrangement of Aβ.

Our observation that Aβ disrupts lipid membranes by two distinct mechanisms is consistent with reports of heterogeneous channel populations based on conductivity measurements (*13*, *24*, *37*). For example, Kourie et al. used electrical conductivity measurements of Aβ bound to lipid membranes and reported dramatically heterogeneous conductance and gating characteristics (*37*, *38*). The ability of membrane active peptides to form oligomers with different permeabilization capabilities has previously been observed with the antimicrobial peptide cecropin which allows the conductance of ions at peptide concentrations lower than those necessary for the passage of larger molecules such as β-galactosidase (*39*). High protein/lipid ratios have also been reported to facilitate incorporation of Aβ into the hydrophobic region of the membrane resulting in membrane thinning, and the subsequent reduction of the dielectric barrier to ion translocation (*29*, *56*).

Our measurements, however, show conductivity arising when distinct peptide aggregates are bound to the membrane as seen in the low-concentration data of Figure 4. It is possible, though, that the large class 3 structures produce large-scale membrane "thinning". It is important also to note that at physiologically relevant concentrations of Aβ [this peptide has been shown to

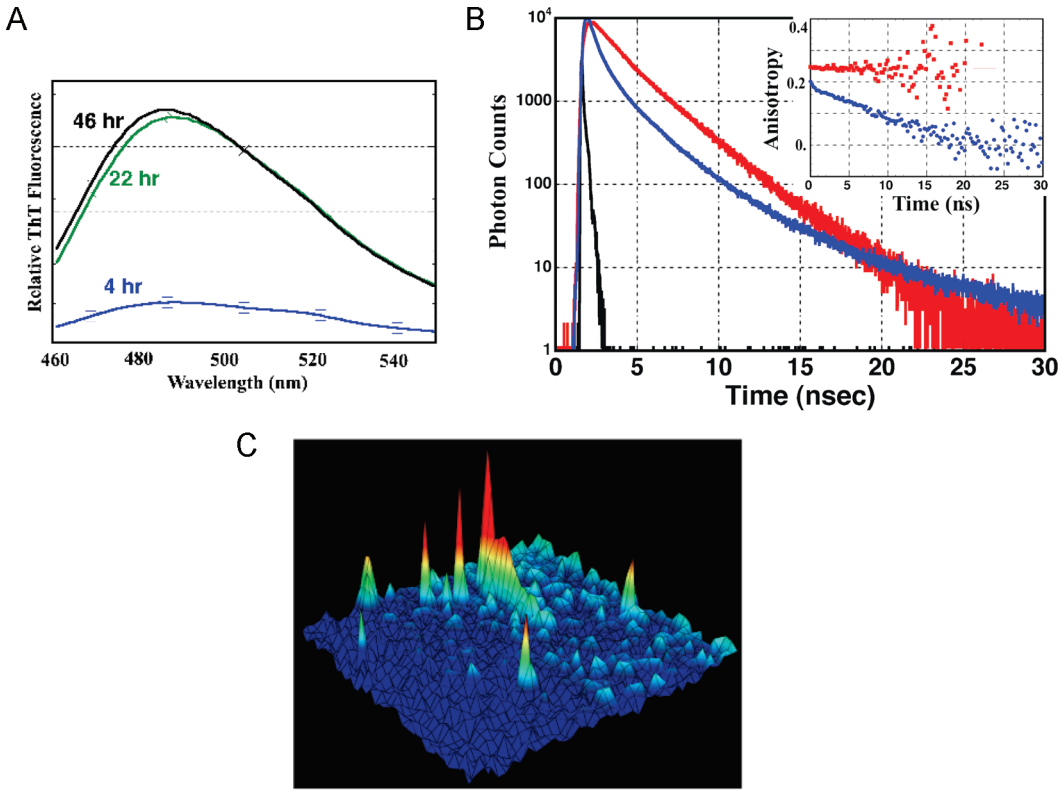

FIGURE 5: Interaction of Aβ with BLM followed by ThT binding. (A) Steady state fluorescence of 2 μM ThT (excitation at 440 nm) freshly added with Aβ40 incubated for 4, 22, and 46 h at 37 °C in 10 mM sodium phosphate and 100 mM sodium chloride (pH 7.4). (B) Time-resolved fluorescence decay and time-resolved anisotropy of ThT added to Aβ after 4 (blue) and 46 h (red) in solution. Excitation of ThT was at 425 nm, with emission monitored at 480 nm. The formation of Aβ fibrils is indicated by the large increase in the ThT fluorescence lifetime (and quantum yield) and the time-independent anisotropy decay reflecting a rotational correlation time in excess of the fluorescence decay window (> 50 ns rotational correlation time). The ThT binding species at 4 h is best fit with a rotational correlation time of 15 ns. (C) ThT binding to unlabeled Aβ40 on a 40 μm × 40 μm BLM. Fresh Aβ40 was incubated with the membrane for 10 min, and ThT (5 μM) was added. The conductivity of the BLM was 20 pS.

form toxic species at concentrations as low as 10 nM (*34*, *57*)], we observe only class 2 aggregates on the membrane, and these discrete species are thus most likely the relevant ones at physiological Aβ40 concentrations.

A critical, and hitherto unresolved, question is whether membrane permeabilizing Aβ species evolve on the phospholipid membrane (*16*) or develop in solution and subsequently bind to the membrane. Numerous studies have shown that the formation of β-sheet rich amyloid fibril by Aβ40 is preceded by a complex series of peptide aggregation events that take place in solution and involve soluble Aβ40 oligomers (*58*−*60*). While in solution Aβ oligomers contain relatively little β-structure, it has been suggested that the membrane-bound toxic forms of Aβ adopt a β-sheet structure (*61*−*63*). An increase in ThT fluorescence supports this hypothesis since an increased fluorescence of this dye reflects binding to the β-sheet of amyloid fibrils (*64*) or protofibrils (*6*).

The results of this study demonstrate that the interaction of Aβ with phospholipid membranes involves distinct and potentially competing mechanisms of formation of oligomers and membrane permeabilization. The monomeric species do not induce any measurable conductance. We also observed membrane-bound Aβ dimers; however, under the experimental conditions used in our study, these did not induce measurable conductivity in the membrane. The neurotoxicity of the dimeric species reported by Shankar et al. (*49*) may, of course, be due to differences between the model membrane used here and the cellular membrane, or it is possible that in vivo dimers and trimers (*50*) may more readily assemble into larger conducting species on the cell membrane. Alternatively, the neurotoxicity reported in ref *49* may be due to a mechanism other than membrane permeabilization.

The membrane disruption by the extended class 3 structure resembles the one observed for antimicrobial peptides termed the "Carpet Mechanism" [SMH model, or the "self-promoted uptake" of Hancock (*65*)], where the antimicrobial peptide carpets the bilayer leading to sequestration of lipids in a detergent-like interaction (*65*, *66*). Peptides that interact with membranes through the SMH mechanism generally do so at micromolar concentrations (*66*), well above physiological levels for Aβ. Hence, the discrete small membrane permeabilizing species and the more extended membrane disrupting structures seen by us may be initiated and facilitated under different conditions.

An extended model presented by Sokolov et al. (*56*) describes an Aβ−membrane interaction reminiscent of that of the SMH membrane disrupting mechanism. The SMH, or self-promoted uptake, model describes a process whereby a protein homogeneously carpets a membrane surface, disrupting membrane structure and increasing membrane conductance. Our observation of the time course for aggregate evolution on the BLM (Figure 4) revealed a dynamic rearrangement of the fluorescence intensity suggestive of a lateral mobility of Aβ-HL488 to be recruited into a structure associated with enhanced ionic conductivity. The question of whether the extended disrupted membrane structures are derived from the coalescence of discrete pores or recruitment of monomeric membrane-bound Aβ-HL488 remains unresolved.

Our observation of binding of Aβ to the membrane and the rapid appearance of β-structured ion-conducting oligomers (relative to the oligomerization rate in solution) is in line with Huang's two-state model. This model describes a process whereby antimicrobial peptides develop pores by a process initiated by monomer binding to the membrane surface followed by surface diffusion and subsequent assembly into discrete pore structures (*54*). In the case of Aβ, β-sheet interactions in an oligomer may be required to stabilize the structure and to provide stability against dissociation back to monomers once it binds to the membrane.

Interestingly, there is a major difference in the background of the images seen in panels B and C of Figure 3 in the transition from uniform and highly diffusive binding to the formation of small oligomers. Namely, the background level shows a significant increase in the fluorescence fluctuations. The intensity peaks are not large enough to correspond to the dimers seen in the large stationary peaks but are larger than expected for monomers. Since the images in this work were obtained by raster scanning (50 ms/pixel) and are not wide field images, rapidly diffusing species may produce lower-intensity peaks due to movement of the chromophore through the observation point. Therefore, our explanation is that these fluctuations correspond to small oligomers that have either associated briefly reducing their mobility and then dissociated or simply continued to diffuse on the surface with reduced mobility and have not yet inserted into the membrane and become fixed (as have the dimers and larger oligomers that are shown as strong peaks in the data). Additional work is necessary to correlate the degree of membrane permeabilization with oligomer size and mobility.

In summary, we observed interaction of Aβ with BLMs ranging from a mechanically stabilizing and nonconductive interaction at low peptide concentrations to the formation of discrete low-conductance structures at physiologically relevant concentrations and, ultimately at higher concentrations, more delocalized high-conductance structures. Our results show that the variations seen in in vitro experiments may reflect a critical dependence on experimental conditions and parameters.

REFERENCES

1. Kirkitadze, M. D., Condron, M. M., and Teplow, D. B. (2001) Identification and characterization of key kinetic intermediates in amyloid β-protein fibrillogenesis. *J. Mol. Biol. 312*, 1103–1119.
2. Wang, S. S., Tobler, S. A., Good, T. A., and Fernandez, E. J. (2003) Hydrogen exchange-mass spectrometry analysis of β-amyloid peptide structure. *Biochemistry 42*, 9507–9514.
3. Lomakin, A., Teplow, D. B., Kirschner, D. A., and Benedek, G. B. (1997) Kinetic theory of fibrillogenesis of amyloid β-protein. *Proc. Natl. Acad. Sci. U.S.A. 94*, 7942–7947.
4. Hou, L., Shao, H., Zhang, Y., Li, H., Menon, N. K., Neuhaus, E. B., Brewer, J. M., Byeon, I. J., Ray, D. G., Vitek, M. P., Iwashita, T., Makula, R. A., Przybyla, A. B., and Zagorski, M. G. (2004) Solution NMR studies of the Aβ(1−40) and Aβ(1−42) peptides establish that the Met35 oxidation state affects the mechanism of amyloid formation. *J. Am. Chem. Soc. 126*, 1992–2005.
5. Dahlgren, K. N., Manelli, A. M., Stine, W. B., Jr., Baker, L. K., Krafft, G. A., and LaDu, M. J. (2002) Oligomeric and fibrillar species of amyloid-β peptides differentially affect neuronal viability. *J. Biol. Chem. 277*, 32046–32053.
6. Walsh, D. M., Hartley, D. M., Kusumoto, Y., Fezoui, Y., Condron, M. M., Lomakin, A., Benedek, G. B., Selkoe, D. J., and Teplow, D. B. (1999) Amyloid β-protein fibrillogenesis. Structure and biological activity of protofibrillar intermediates. *J. Biol. Chem. 274*, 25945–25952.
7. Caughey, B., and Lansbury, P. T. (2003) Protofibrils, pores, fibrils, and neurodegeneration: Separating the responsible protein aggregates from the innocent bystanders. *Annu. Rev. Neurosci. 26*, 267–298.
8. Arispe, N., Pollard, H. B., and Rojas, E. (1993) Giant multilevel cation channels formed by Alzheimer disease amyloid β-protein [AβP-(1−40)] in bilayer membranes. *Proc. Natl. Acad. Sci. U.S.A. 90*, 10573–10577.
9. Arispe, N., Pollard, H. B., and Rojas, E. (1994) β-Amyloid Ca^{2+}-channel hypothesis for neuronal death in Alzheimer disease. *Mol. Cell. Biochem. 140*, 119–125.
10. Kayed, R., Head, E., Thompson, J. L., McIntire, T. M., Milton, S. C., Cotman, C. W., and Glabe, C. G. (2003) Common structure of soluble amyloid oligomers implies common mechanism of pathogenesis. *Science 300*, 486–489.
11. Lashuel, H. A., and Lansbury, P. T., Jr. (2006) Are amyloid diseases caused by protein aggregates that mimic bacterial pore-forming toxins? *Q. Rev. Biophys. 39*, 167–201.
12. Kawahara, M., Kuroda, Y., Arispe, N., and Rojas, E. (2000) Alzheimer's β-amyloid, human islet amylin, and prion protein fragment evoke intracellular free calcium elevations by a common mechanism in a hypothalamic GnRH neuronal cell line. *J. Biol. Chem. 275*, 14077–14083.
13. Kagan, B. L., Hirakura, Y., Azimov, R., Azimova, R., and Lin, M. C. (2002) The channel hypothesis of Alzheimer's disease: Current status. *Peptides 23*, 1311–1315.
14. Harper, J. D., and Lansbury, P. T., Jr. (1997) Models of amyloid seeding in Alzheimer's disease and scrapie: Mechanistic truths and physiological consequences of the time-dependent solubility of amyloid proteins. *Annu. Rev. Biochem. 66*, 385–407.
15. Demuro, A., Mina, E., Kayed, R., Milton, S. C., Parker, I., and Glabe, C. G. (2005) Calcium dysregulation and membrane disruption as a ubiquitous neurotoxic mechanism of soluble amyloid oligomers. *J. Biol. Chem. 280*, 17294–17300.
16. Kagan, B. L., Azimov, R., and Azimova, R. (2004) Amyloid peptide channels. *J. Membr. Biol. 202*, 1–10.
17. Quist, A., Doudevski, I., Lin, H., Azimova, R., Ng, D., Frangione, B., Kagan, B., Ghiso, J., and Lal, R. (2005) Amyloid ion channels: A common structural link for protein-misfolding disease. *Proc. Natl. Acad. Sci. U.S.A. 102*, 10427–10432.
18. Suh, Y. H., and Checler, F. (2002) Amyloid precursor protein, presenilins, and α-synuclein: Molecular pathogenesis and pharmacological applications in Alzheimer's disease. *Pharmacol. Rev. 54*, 469–525.
19. Rhee, S. K., Quist, A. P., and Lal, R. (1998) Amyloid β protein-(1−42) forms calcium-permeable, Zn^{2+}-sensitive channel. *J. Biol. Chem. 273*, 13379–13382.
20. Kawahara, M., and Kuroda, Y. (2000) Molecular mechanism of neurodegeneration induced by Alzheimer's β-amyloid protein: Channel formation and disruption of calcium homeostasis. *Brain Res. Bull. 53*, 389–397.
21. Isaacs, A. M., Senn, D. B., Yuan, M., Shine, J. P., and Yankner, B. A. (2006) Acceleration of amyloid β-peptide aggregation by physiological concentrations of calcium. *J. Biol. Chem. 281*, 27916–27923.
22. Arispe, N., and Doh, M. (2002) Plasma membrane cholesterol controls the cytotoxicity of Alzheimer's disease AβP (1−40) and (1−42) peptides. *FASEB J. 16*, 1526–1536.
23. Mclaurin, J., Cecal, R., Kierstead, M. E., Tian, X., Phinney, A. L., Manea, M., French, J. E., Lambermon, M. H. L., Darabie, A. A., Brown, M. E., Janus, C., Chishti, M. A., Horne, P., Westway, D., Fraser, P. E., Mount, H. T. J., Przybylski, M., and St George-Hyslop, P. (2002) Therapeutically effective antibodies against amyloid-B peptide target amyloid-β 4−10 and inhibit cytotoxicity and fibrillogenesis. *Nat. Med. 8*, 1263–1269.
24. Simakova, O., and Arispe, N. J. (2006) Early and late cytotoxic effects of external application of the Alzheimer's Aβ result from the initial formation and function of Aβ ion channels. *Biochemistry 45*, 5907–5915.
25. Dalla Serra, M., and Menestrina, G. (2003) Liposomes in the study of pore-forming toxins. *Methods Enzymol. 372*, 99–124.
26. Del Mar Martinez-Senac, M., Villalain, J., and Gomez-Fernandez, J. C. (1999) Structure of the Alzheimer β-amyloid peptide (25−35) and its interaction with negatively charged phospholipid vesicles. *Eur. J. Biochem. 265*, 744–753.
27. Alarcon, J. M., Brito, J. A., Hermosilla, T., Atwater, I., Mears, D., and Rojas, E. (2006) Ion channel formation by Alzheimer's disease amyloid β-peptide (Aβ40) in unilamellar liposomes is determined by anionic phospholipids. *Peptides 27*, 95–104.
28. Arispe, N. (2004) Architecture of the Alzheimer's AβP ion channel pore. *J. Membr. Biol. 197*, 33–48.
29. Kayed, R., Sokolov, Y., Edmonds, B., McIntire, T. M., Milton, S. C., Hall, J. E., and Glabe, C. G. (2004) Permeabilization of lipid bilayers is a common conformation-dependent activity of soluble amyloid oligomers in protein misfolding diseases. *J. Biol. Chem. 279*, 46363–46366.

30. Ravault, S., Soubias, O., Saurel, O., Thomas, A., Brasseur, R., and Milon, A. (2005) Fusogenic Alzheimer's peptide fragment Aβ(29−42) in interaction with lipid bilayers: Secondary structure, dynamics, and specific interaction with phosphatidyl ethanolamine polar heads as revealed by solid-state NMR. *Protein Sci. 14*, 1181–1189.
31. Lin, M. C., and Kagan, B. L. (2002) Electrophysiologic properties of channels induced by Aβ25−35 in planar lipid bilayers. *Peptides 23*, 1215–1228.
32. Huang, T. H., Yang, D. S., Plaskos, N. P., Go, S., Yip, C. M., Fraser, P. E., and Chakrabartty, A. (2000) Structural studies of soluble oligomers of the Alzheimer β-amyloid peptide. *J. Mol. Biol. 297*, 73–87.
33. Losic, D., Martin, L. L., Mechler, A., Aguilar, M. I., and Small, D. H. (2006) High resolution scanning tunnelling microscopy of the β-amyloid protein (Aβ1−40) of Alzheimer's disease suggests a novel mechanism of oligomer assembly. *J. Struct. Biol. 155*, 104–110.
34. Stine, W. B., Jr., Dahlgren, K. N., Krafft, G. A., and LaDu, M. J. (2003) In vitro characterization of conditions for amyloid-β peptide oligomerization and fibrillogenesis. *J. Biol. Chem. 278*, 11612–11622.
35. Soto, C., Castano, E. M., Frangione, B., and Inestrosa, N. C. (1995) The α-helical to β-strand transition in the amino-terminal fragment of the amyloid β-peptide modulates amyloid formation. *J. Biol. Chem. 270*, 3063–3067.
36. Tycko, R. (2003) Insights in the amyloid folding problem from solid-state NMR. *Biochemistry 42*, 3151–3159.
37. Kourie, J. I., Culverson, A. L., Farrelly, P. V., Henry, C. L., and Laohachai, K. N. (2002) Heterogeneous amyloid-formed ion channels as a common cytotoxic mechanism: Implications for therapeutic strategies against amyloidosis. *Cell Biochem. Biophys. 36*, 191–207.
38. Kourie, J. I., Henry, C. L., and Farrelly, P. (2001) Diversity of amyloid β protein fragment [1−40]-formed channels. *Cell. Mol. Neurobiol. 21*, 255–284.
39. Sato, H., and Feix, J. B. (2006) Peptide-membrane interactions and mechanisms of membrane destruction by amphipathic α-helical antimicrobial peptides. *Biochim. Biophys. Acta 1758*, 1245–1256.
40. Arispe, N., Pollard, H. B., and Rojas, E. (1996) Zn^{2+} interaction with Alzheimer amyloid β protein calcium channels. *Proc. Natl. Acad. Sci. U.S.A. 93*, 1710–1715.
41. Gorman, P. M., Yip, C. M., Fraser, P. E., and Chakrabartty, A. (2003) Alternate aggregation pathways ofthe Alzheimer β-amyloid peptide: Association kinetics at endosomal pH. *J. Mol. Biol. 325*, 743–757.
42. Fezoui, Y., Hartley, D. M., Harper, J. D., Khurana, R., Walsh, D. M., Condron, M. M., Selkoe, D. J., Lansbury, P. T., Jr., Fink, A. L., and Teplow, D. B. (2000) An improved method of preparing the amyloid β-protein for fibrillogenesis and neurotoxicity experiments. *Amyloid 7*, 166–178.
43. Kawahara, M., and Kuroda, Y. (2001) Intracellular calcium changes in neuronal cells induced by Alzheimer's β-amyloid protein are blocked by estradiol and cholesterol. *Cell. Mol. Neurobiol. 21*, 1–13.
44. Klein, W. L., Stine, W. B., Jr., and Teplow, D. B. (2004) Small assemblies of unmodified amyloid β-protein are the proximate neurotoxin in Alzheimer's disease. *Neurobiol. Aging 25*, 569–580.
45. Ide, T., Takeuchi, Y., and Yanagida, T. (2002) Development of an experimental apparatus for simultaneous observation of optical and electrical signals from single ion channels. *Single Mol. 3*, 33–42.
46. O'Connor, D., and Phillips, D. (1984) Time-Correlated Single Photon Counting, Academic Press, London.
47. Ding, H., Wong, P. T., Lee, E. L., Gafni, A., and Steel, D. G. (2009) Determination of the oligomer size of amyloidogenic protein β-amyloid(1−40) by single-molecule spectroscopy. *Biophys. J. 97*, 912–921.
48. Kremer, J. J., and Murphy, R. M. (2003) Kinetics of adsorption of β-amyloid peptide Aβ(1−40) to lipid bilayers. *J. Biochem. Biophys. Methods 57*, 159–169.
49. Shankar, G. M., Li, S., Mehta, T. H., Garcia-Munoz, A., Shepardson, N. E., Smith, I., Brett, F. M., Farrell, M. A., Rowan, M. J., Lemere, C. A., Regan, C. M., Walsh, D. M., Sabatini, B. L., and Selkoe, D. J. (2008) Amyloid-β protein dimers isolated directly from Alzheimer's brains impair synaptic plasticity and memory. *Nat. Med. 14*, 837–842.
50. Selkoe, D. J. (2008) Soluble oligomers of the amyloid β-protein impair synaptic plasticity and behavior. *Behav. Brain Res. 192*, 106–113.
51. Terzi, E., Holzemann, G., and Seelig, J. (1997) Interaction of Alzheimer β-amyloid peptide(1−40) with lipid membranes. *Biochemistry 36*, 14845–14852.
52. Wong, P. T., Schauerte, J. A., Wisser, K. C., Ding, H., Lee, E. L., Steel, D. G., and Gafni, A. (2009) Amyloid-membrane binding and permeabilization are distinct processes influenced by membrane charge and fluidity. *J. Mol. Biol. 386*, 81–96.
53. Segrest, J. P., Pownall, H. J., Jackson, R. L., Glenner, G. G., and Pollock, P. S. (1976) Amyloid A: Amphipathic helixes and lipid binding. *Biochemistry 15*, 3187–3191.
54. Huang, H. W. (2000) Action of antimicrobial peptides: Two-state model. *Biochemistry 39*, 8347–8352.
55. Lee, M. T., Chen, F. Y., and Huang, H. W. (2004) Energetics of pore formation induced by membrane active peptides. *Biochemistry 43*, 3590–3599.
56. Sokolov, Y., Kozak, J. A., Kayed, R., Chanturiya, A., Glabe, C., and Hall, J. E. (2006) Soluble amyloid oligomers increase bilayer conductance by altering dielectric structure. *J. Gen. Physiol. 128*, 637–647.
57. Yankner, B. A., Duffy, L. K., and Kirschner, D. A. (1990) Neurotrophic and neurotoxic effects of amyloid β protein: Reversal by tachykinin neuropeptides. *Science 250*, 279–282.
58. Baskakov, I. V., Legname, G., Baldwin, M. A., Prusiner, S. B., and Cohen, F. E. (2002) Pathway complexity of prion protein assembly into amyloid. *J. Biol. Chem. 277*, 21140–21148.
59. Bitan, G., Kirkitadze, M. D., Lomakin, A., Vollers, S. S., Benedek, G. B., and Teplow, D. B. (2003) Amyloid β-protein (Aβ) assembly: Aβ40 and Aβ42 oligomerize through distinct pathways. *Proc. Natl. Acad. Sci. U.S.A. 100*, 330–335.
60. Tomski, S. J., and Murphy, R. M. (1992) Kinetics of aggregation of synthetic β-amyloid peptide. *Arch. Biochem. Biophys. 294*, 630–638.
61. Soto, C., Castano, E. M., Kumar, R. A., Beavis, R. C., and Frangione, B. (1995) Fibrillogenesis of synthetic amyloid-β peptides is dependent on their initial secondary structure. *Neurosci. Lett. 200*, 105–108.
62. Singer, S. J., and Dewji, N. N. (2006) Evidence that Perutz's double-β-stranded subunit structure for β-amyloids also applies to their channel-forming structures in membranes. *Proc. Natl. Acad. Sci. U.S.A. 103*, 1546–1550.
63. Pike, C. J., Walencewicz-Wasserman, A. J., Kosmoski, J., Cribbs, D. H., Glabe, C. G., and Cotman, C. W. (1995) Structure-activity analyses of β-amyloid peptides: Contributions of the β25−35 region to aggregation and neurotoxicity. *J. Neurochem. 64*, 253–265.
64. LeVine, H., III (1993) Thioflavine T interaction with synthetic Alzheimer's disease β-amyloid peptides: Detection of amyloid aggregation in solution. *Protein Sci. 2*, 404–410.
65. Hwang, P. M., and Vogel, H. J. (1998) Structure-function relationships of antimicrobial peptides. *Biochem. Cell Biol. 76*, 235–246.
66. Zasloff, M. (2002) Antimicrobial peptides of multicellular organisms. *Nature 415*, 389–395.